The Relationship between Total Area Divergence and Convective Precipitation in South Florida

ANDREW I. WATSON AND DAVID O. BLANCHARD

Weather Research Program,[1] Environmental Research Laboratories, NOAA, Boulder, CO 80303

(Manuscript received 22 April 1983, in final form 24 January 1984)

ABSTRACT

Total area divergence is related to area rainfall using data collected during the Florida Area Cumulus Experiment (FACE) 1975 field experiment over a network that covered 1440 km^2. A convergence event is defined as a monotonic decrease in total area divergence of more than 25×10^{-6} s^{-1} for more than ten minutes. This change in total area divergence is related to the total amount of area rainfall considered to be associated with the convergence event. For 121 convergence events during July and August 1975, a correlation coefficient of -0.59 is found between change in convergence and rainfall amount. When the ensemble is subdivided, it is found that for slow moving convective systems, or when low-level winds are weak, there is twice the amount of rainfall per convergence event. When middle-level (850–500 mb) relative humidity is in the range 50–65%, the correlation coefficient between convergence and rainfall is -0.81. Data are also partitioned according to stability and buoyancy. Convective outflow and its reflection in total area divergence are examined, and relationships are developed for determining the amount of precipitation for each divergence event. For the 75 rain events during FACE 1975, a correlation coefficient of 0.75 is found between the change in divergence and the rainfall amount.

1. Introduction

The idea that surface convergence and convective rainfall are related is not new. The classic Thunderstorm Project in the late 1940s reported the relationship between convergence and cumulus cloud development. Byers and Rodebush (1948) found that low-level subsynoptic-scale convergence formed by the sea-breeze circulation is the probable cause of afternoon thunderstorms across the Florida peninsula. Byers and Braham (1949) found mesoscale convergence at the surface up to 30 minutes before the appearance of a radar echo. Gentry and Moore (1954) hypothesized that the locations of summer showers in southeast Florida are controlled by areas of convergence forced by the sea breeze which in turn responds to the direction and speed of the low-level winds. They showed a general relationship between the 1500-m wind speed and direction from the Miami sounding and the occurrence of precipitation in the Miami area. More recently, Burpee (1979) examined peninsula-scale convergence and found much more net convergence on dry sea-breeze days than on rainy sea-breeze days. The increased thunderstorm activity produces rain, cool outflows, and broad cirrus shields that reduce the thermal forcing of the sea-breeze circulation which, in turn, decreases convergence during the late afternoon on days with extensive rainfall. Burpee also found that greater amounts of precipitation occurred on sea-breeze days when midtropospheric moisture was large. Cooper *et al.* (1982) reported that the initial triggering of convection over south Florida is indeed related to peninsula-scale convergence. They found that even after peninsula-scale convergence has reached its peak, there is a convective-scale feedback where surface outflows generate surface convergence areas. These areas, in turn, initiate new cells.

Many modeling efforts have shown that low-level convergence has a significant effect on cumulus convection. Pielke (1974) developed a three-dimensional sea-breeze numerical model without latent heat release that closely simulates the initial response of convection over south Florida. He showed that the sea-breeze convergence patterns are the primary control of the general locations of the initial cloud and shower complexes. Tripoli and Cotton (1980) varied the amounts of convergence beneath their three-dimensional cloud model and concluded that the intensity of a cumulonimbus system is primarily related to the amount of moist static energy supplied to the storm by mesoscale convergence when low-level shear is relatively weak.

In the realm of prediction and nowcasting, Day (1953) had limited success in correlating area divergence from a pibal triangle over southeast Florida and adjacent waters with summertime convective precipitation in the Miami area. More recently and on a

[1] A major portion of this research was conducted while the authors were at the National Hurricane and Experimental Meteorology Laboratory, NOAA, Coral Gables, Florida.

smaller scale, Ulanski and Garstang (1978), using Florida Area Cumulus Experiment (FACE) 1971 and 1973 data, found readily identifiable convergence zones that, at times, preceded the onset of precipitation by as much as 60–90 min. They related the convergence gradient to maximum point rainfall when cells of convergence had contours $\geq 600 \times 10^{-6}$ s^{-1} and persisted for 15 min or more. Ulanski and Garstang omitted days when rainfall totaled less than 2 mm or synoptic conditions were considered disturbed.

We show here a relationship between convergence and rainfall on an area-wide (meso-β) basis using a large set of data. Only divergence in the form of an area-averaged divergence (total area divergence) over the entire mesonetwork is presented, as contrasted with the cellular approach of Ulanski and Garstang. An ensemble approach is employed to document the total area divergence–area precipitation relationships. FACE 1975 mesonetwork data are used to develop the statistical relationships. Precipitation volumes are derived by radar estimation and adjusted by a smaller raingage network.

2. Data and analysis

a. FACE 1975 mesonetwork

The mesoscale program of FACE 1975 was a major field effort designed to help determine the interaction of both seeded and natural clouds with each other and with their environment. The FACE 1975 field project was conducted from 1 July through 31 August in the area of south Florida shown in Fig. 1. A description of all data collected in FACE 1975 is given by Staff, Cumulus Group (1976). The field network was divided into two coincident networks, the raingage and the mesoscale. The 66 raingages were spaced 3.2 km apart and covered 598 km^2. The mesoscale network covered 1440 km^2 and measured surface wind (at 4 m), pressure, temperature, and relative humidity. The network consisted of 46 surface stations, 6.4 km apart in a 32 $\times$ 45 km area.

b. Data reduction techniques

The wind information was recorded primarily on strip charts and digitized in 5-min time intervals. For this study, 56 days were analyzed: 1–26 July and 1–30 August. Because south Florida summertime convection is generated mainly by differential heating between water and land surfaces, only data from 0800 to 2000 Eastern Daylight Time (EDT) were reduced. Through the use of an objective analysis scheme, the mesonetwork wind data were transformed into a uniform grid of divergence values. The objective analysis scheme was basically a Cressman (1959) technique. A 6 $\times$ 8 grid of equally spaced (6.4 km) grid points (see Fig. 1) was superimposed upon the original network. The u- and v-components for each grid point were estimated from an initial guess derived from a distance-weighted average for the two closest reporting stations. The value of the first guess at a grid point was corrected according to the value of the data at the reporting stations within the radius of influence (r = 9.7 km). Since most of the sites were at, or very close to, the grid points, only a single pass was made through the field of data with the objective analysis scheme. The values of u- and v-components at each of the grid points were then used to compute the divergence quantities using a centered finite-difference scheme.

Area precipitation totals were derived by radar and adjusted by the FACE raingage network. The major consideration in choosing radar over raingages was the fact that the areal coverage of the raingage network (598 km^2) was considerably less than the areal coverage of the wind network (1440 km^2). The reduction in area of the wind network necessary to match the area of the raingages was deemed undesirable.

Radar data were obtained from the WSR-57 operated by the National Hurricane Center in Coral Gables, approximately 110 km southeast of the wind network. The returned radar power from a scan every 5 min was digitized and written onto magnetic tape. Occasional data gaps occurred. For small data gaps (15 min or less), the next usable radar scan was assumed adequate for the entire period. For large gaps, the data were considered missing and no rainfall estimates were determined.

The radar data were "cleaned up" as much as possible. The methods included range normalization, an examination of the noise levels, establishment of range bias of reflectivity, and removal of periods of anomalous propagation.

The rainfall analysis procedure involved the adjustment of radar estimates of rainfall with actual raingage data (Woodley *et al.*, 1975). A gage-to-radar rainfall ratio G/R was used for adjusting radar values; G was found by summing the gage rainfall in the FACE 1975 raingage network and dividing the sum by the number of reporting gages, and R is the sum of the 5-min radar-derived rainfall values for the raingage network, using the Z–R relationship

$$Z = 300R^{1.4} \tag{1}$$

that was used throughout the FACE experiments (Woodley and Herndon, 1970). Then R is divided by the area for the same time period as G. A daily G/R value was calculated using all time periods when there was rainfall recorded by the raingages and when radar data were available. Adjusted radar rainfall was obtained by multiplying the unadjusted value by G/R. On days when $G < 1$ mm, G/R was not applied; for those days, G/R was set equal to 1.

Radar was also used to estimate the beginning and ending times of rain. The beginning of rain was estimated as the time when greater than 0.01 mm radar-estimated area rainfall first occurred in a 5 min period.

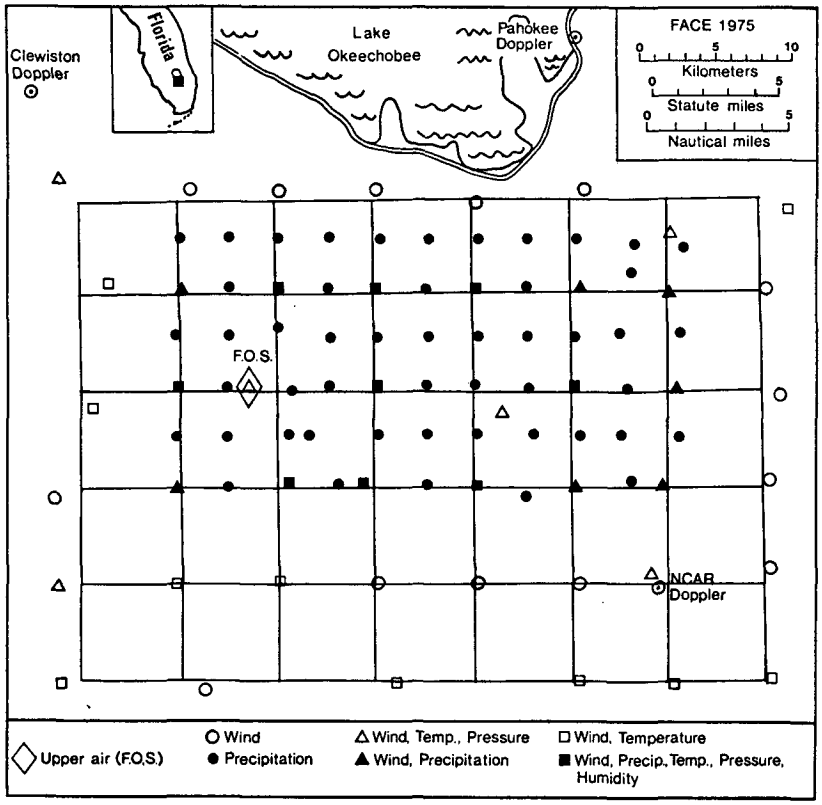

FIG. 1. The FACE 1975 mesonetwork. The raingage cluster is identified by the solid circles.

The ending time of rainfall occurred when rainfall fell below this value. Results from this technique appeared to relate well to precipitation which was recorded in the smaller FACE raingage network.

c. *Divergence quantities*

Area-averaged divergence can be calculated in several different ways. Cunning *et al.* (1982) have called that quantity "Total-Area-Divergence," DIV_T, and have defined it as

$$\mathrm{DIV}_T = N_T^{-1} \sum_{i=1}^{N_T} (\nabla_H \cdot \mathbf{V})_i \qquad (2)$$

for each 5 min period, where N_T is the total number of grid points in the network and $\nabla_H \cdot \mathbf{V}$ is the magnitude of the horizontal divergence at each grid point. This definition of DIV_T is being used here; DIV_T is the same as the line integral of the normal component of the wind around the network boundary divided by the area of the network. Two other quantities that are related to development and dissipation of deep convection are weighted convergence and weighted divergence. Weighted convergence is the summation of only convergence values at grid points divided by the total number of grid points for each 5-min period. Weighted divergence, the opposite of weighted convergence, relies on only grid points with positive divergence values. The sum of weighted convergence and weighted divergence is total area divergence. Weighted convergence filters out positive divergence whereas the inverse is true for weighted divergence. These quantities require an inner grid where positive and negative divergence quantities are calculated.

Figure 2 shows sample profiles of total area divergence, weighted convergence and divergence, and radar-derived rainfall for 3 August 1975. Mean rain depth is defined as the amount of area rainfall that has accumulated in a 5-min period. The sinusoidal pattern of total area divergence is typical for rainfall events. The convergence stage is related to inflow and the development of the storm. This stage ends at peak convergence and the first detection of precipitation on the surface. The divergence stage is associated with downdrafts, outflow at the surface, a maximum in precipitation followed by a maximum in divergence, and eventual dissipation of the system within the mesonetwork. A more detailed discussion of the total area divergence–rainfall patterns may be found in Cooper *et al.* (1982).

Because surface convergence identifies convective potential that is forced from the boundary layer, the boundary layer must be sufficiently mixed so that po-

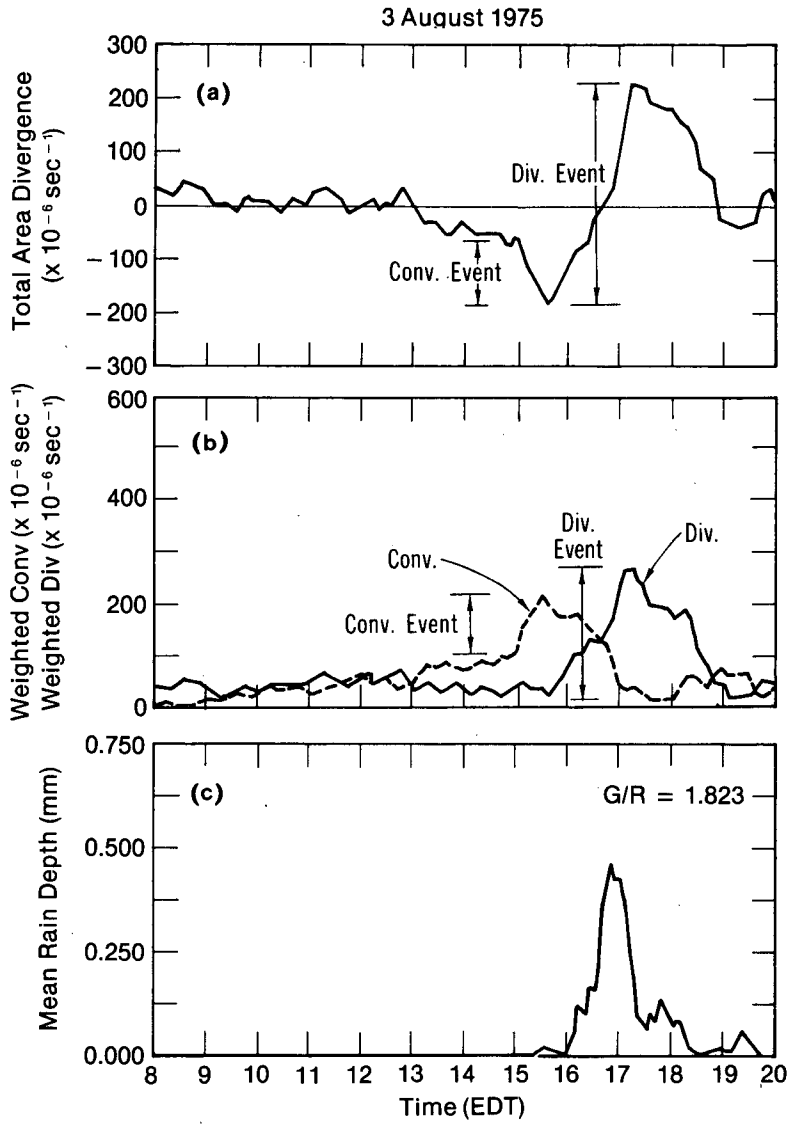

FIG. 2. Total area divergence (a), weighted convergence and divergence (b), and rainfall profiles (c) for 3 August 1975.

tential temperature, mixing ratio, and momentum remain relatively constant. A mixed boundary layer was identified by means of rawinsonde information and ground-based photography. Three soundings were taken at 1100, 1400, and 1700 EDT at the Field Observing Site (FOS, Fig. 1) whenever possible. This method was limited since it yielded information only at one point at a particular time. The predominant method used photography. A panorama of the entire horizon up to an elevation angle exceeding 60° was taken at half-hour intervals between 1000 and 1800 EDT each day at FOS. Mixing was then determined visually by observing the formation of cumulus or stratocumulus. Some 29 periods during the 56 days were considered insufficiently mixed. Most of these periods occurred after 1600 EDT under thunderstorm outflow conditions.

3. Interpretation of divergence–rainfall relationships

This section is devoted to the development of the relationship between total area divergence and convective precipitation. Presentation of the technique for defining a convergence event is followed by a discussion of the statistical results. The relationship between outflow divergence and precipitation is also considered. Definitions of divergence–rainfall terms are included in the Appendix.

a. A convergence event

The sinusoidal pattern shown in the total area divergence time series in Fig. 2a depicts a convergence period coupled with the development of convection, followed by divergence related to precipitation, outflow, and the demise of the convective system. The con-

vergence portion of the total area divergence time series is used to develop the relationship between convergence and rainfall.

For the purposes of this paper a convergence event is defined, objectively, as a monotonic decrease in total area divergence of more than 25×10^{-6} s^{-1} sustained for more than 10 min. The magnitude of the convergence event (ΔDIV) is the difference between the values at beginning convergence and peak convergence. To filter noise from the evolution of total area divergence with time, this definition is applied to a three-point running mean (15 min average). Sensitivity tests were made in the definition of a convergence event, but it was found that smaller changes created many events that were considered to be noise, and large changes (for example, -50×10^{-6} s^{-1} ΔDIV) missed significant rain events. The same description of a convergence event is also used for weighted convergence.

The boundary layer must be well mixed for surface divergence to be an important tool for identification of convective potential. Therefore, if the boundary layer is not well mixed at the time of a convergence event, the event is eliminated from the sample. If a convergence event occurs in predominantly positive total area divergence, it is assumed that there is insufficient convective forcing to produce precipitation; therefore, the event is also eliminated from the ensemble. For example, the period after maximum divergence (1710–1900 EDT) in Fig. 2a meets the convergence event criteria, but since the event is in predominantly positive total area divergence the event is eliminated. Incidentally, the boundary layer on 3 August was considered insufficiently mixed after 1645 EDT because of thunderstorm outflow. Finally, all convergence events that cross zero total area divergence are assumed to begin at zero divergence, rather than at the initial drop in divergence. In south Florida, 112 events meeting the convergence event criterion of ΔDIV = -25×10^{-6} s^{-1} were eliminated because of the mixed boundary-layer and positive divergence specifications. Nearly all were weak and had little or no precipitation.

As defined by the convergence event criteria, 121 convergence events occurred on 52 of the 56 days analyzed. Two days had no radar data and two days had no convergence events. The two days with no convergence events were considered disturbed, with cold troughs aloft and with middle and high cloudiness suppressing surface heating.

Radar rainfall was corrected by a daily G/R value. Beginning and ending rain was assumed when more/less than 0.01 mm area precipitation was achieved. The rain periods were then coupled with the closest occurring convergence event. Of the 121 convergence events, 75 had related precipitation. No convergence events could be found for 15 rain periods. Only precipitation occurring in the mesonetwork was totaled.

Figure 3 shows how the 121 convergence events are grouped according to the magnitude of convergence and rainfall for FACE 1975. An event not shaded or hatched is indicative of no rain; hatching denotes precipitation totals less than 1 mm. In the interval from -25 to -50×10^{-6} s^{-1} a total of 66 events occur; 41 of the 66 events have no associated precipitation, and seven have significant rainfall totaling more than 1 mm. When the magnitude of the convergence event is greater than -50×10^{-6} s^{-1}, there are only five no-rain events; above -75×10^{-6} s^{-1}, there is only one no-rain event.

Several aspects become apparent when the convergence–rainfall data are examined on an individual event basis (Fig. 3). When the convergence events are weak ($< -50 \times 10^{-6}$ s^{-1}), rainfall varies from no-rain to moderate precipitation; no area rainfall totals exceed 4.9 mm. This can be attributed to factors such as con-

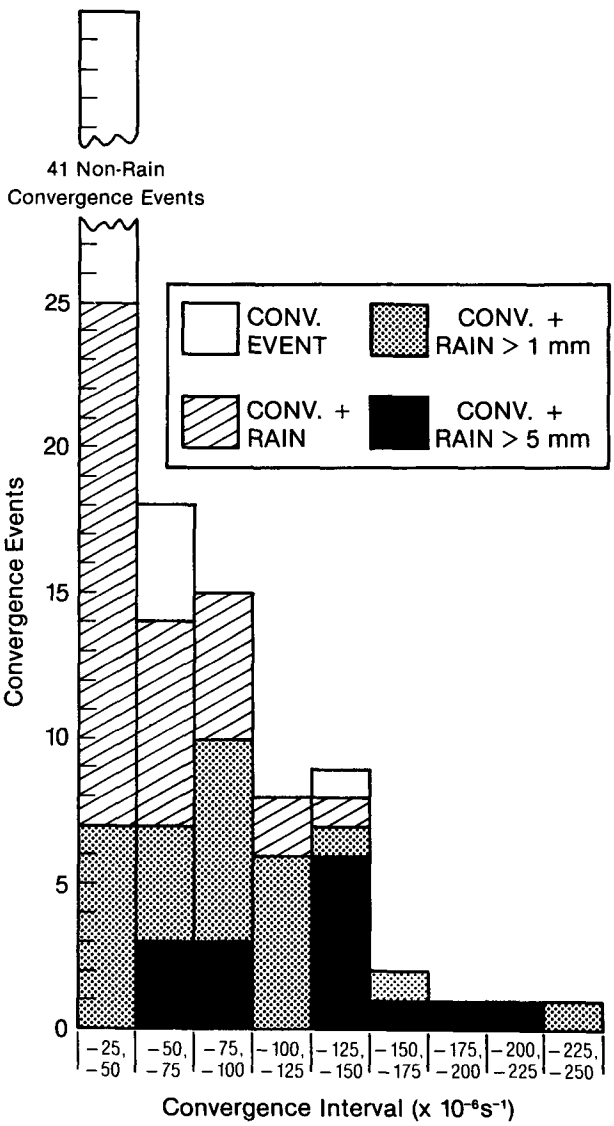

FIG. 3. Frequency distribution of FACE 1975 convergence events in terms of the magnitude of the events. The amount of precipitation per event is also shown.

ditions not being favorable for deep convection, or the occurrence of convergence in the network and rain outside the network. For example, the lake breeze from Lake Okeechobee just north of the network can cause convergence but conditions in the network may not yet be favorable for deep convection. Outflows from distant cumulonimbus systems may traverse the network, causing convergence without triggering new convection.

Variability can also be seen at higher convergence intervals (Fig. 3). The strongest convergence does not always indicate the heaviest rainfall. Natural variability and measurement technique are responsible. Total area divergence is measured from a fixed area, but the sizes of convective systems vary and seldom do they lie entirely within the confines of the network. A system may straddle the boundaries, or only a small portion may lie within the network.

b. *Statistical relationships*

A statistical study of the data illustrates the relationship between convergence and rainfall. All convergence events were determined only by the total area divergence and weighted convergence time series. No distinction was made as to how convergence cells are situated in the mesonetwork.

Table 1 summarizes the results for south Florida. Of the 121 events, 75 had measurable precipitation; the average is 1.78 mm per convergence event. The average rain amount becomes 2.87 mm when only events with rain are considered. A correlation coefficient of −0.59 is found between the change in total area divergence (convergence event) and the related area rainfall amount. A total of 15 rain periods were missed; that is, they occurred without a corresponding convergence signal. Average precipitation during these periods was 1.48 mm. These 15 missed rain periods are not included in the statistical study. The significance (*P*-value) is provided for the statistical comparison of convergence and related precipitation. The significance is the probability of the sample originating from uncorrelated populations. Since the population distributions are non-normal (Fig. 3), there may be some slight statistical errors in the analysis.

When the convergence event threshold is increased to -50×10^{-6} s^{-1} (Table 1), only the larger convergence events are recorded. The data in the leftmost column in Fig. 3 are eliminated and the 25 rain events represented become rain misses (-25 to -50×10^{-6} s^{-1} convergence interval). 50 out of 55 convergence events have rain, but 40 rain periods are not detected by this convergence threshold. There is a significant increase in the average change in area divergence (-99×10^{-6} versus -65×10^{-6} s^{-1}) and average rainfall (3.47 versus 1.78 mm). A noticeable drop in correlation (-0.59 to -0.43) between convergence and rainfall is also recorded because 41 weak convergence events with no rainfall, which are well correlated, are removed from the sample.

To further investigate the interactions of surface convergence and rainfall, the ensemble is partitioned according to several parameters that may be important indicators of rainfall in south Florida. These include

TABLE 1. Total area divergence versus area rainfall, based upon FACE 1975 mesonetwork data. The change in total area divergence threshold is -25×10^{-6} s^{-1} except where stated. $\overline{\Delta DIV}$ is the average change in total area divergence per event.

Criteria	Number of cases	Rain periods	$\overline{\text{Rain}}$ (mm) Rain periods	$\overline{\text{Rain}}$ (mm) All events	$\overline{\Delta DIV}$ ($\times 10^{-6}$ s^{-1})	Correlation coefficient r	Significance	Rain misses Number of events	Rain misses $\overline{\text{Rain}}$ (mm)
All	121	75	2.87	1.78	−65	−0.59	<0.001	15	1.48
$\Delta DIV \leq -50 \times 10^{-6}$ s^{-1}	55	50	3.89	3.47	−99	−0.43	0.001	40	1.14
RH < 50%	47	26	2.68	1.48	−68	−0.43	0.002	2	0.26
50% ≤ RH ≤ 65%	39	28	2.47	1.77	−65	−0.81	<0.001	6	0.89
RH > 65%	35	21	3.65	2.19	−61	−0.66	<0.001	7	2.33
SI > 2	59	39	3.15	2.08	−67	−0.68	<0.001	8	1.16
SI ≤ 2	62	36	2.57	1.49	−63	−0.49	<0.001	7	1.84
BE ≤ 1000 J kg^{-1}	58	35	3.06	1.85	−62	−0.57	<0.001	9	1.75
BE > 1000 J kg^{-1}	63	40	2.71	1.72	−67	−0.63	<0.001	6	1.08
$K < 25$	37	17	3.04	1.40	−68	−0.41	0.011	3	0.23
$25 \leq K \leq 29$	42	35	2.67	2.24	−71	−0.78	<0.001	6	1.61
$K > 29$	42	23	3.03	1.66	−56	−0.60	<0.001	6	1.98
$V_{1\text{-}10} \geq 4$ m s^{-1}	75	40	2.36	1.26	−56	−0.62	<0.001	9	1.85
$V_{1\text{-}10} < 4$ m s^{-1}	46	35	3.46	2.63	−79	−0.53	<0.001	6	0.93
$Dir_{1\text{-}10}$ (360–090°)	38	20	3.20	1.68	−63	−0.63	<0.001	2	0.89
$Dir_{1\text{-}10}$ (090–135°)	44	29	3.07	2.03	−74	−0.60	<0.001	6	1.36
$Dir_{1\text{-}10}$ (135–270°)	39	26	2.40	1.60	−57	−0.59	<0.001	7	1.76

midtropospheric relative humidity (850–500 mb), Showalter stability index SI, *K*-index, net positive buoyant energy BE, and the mean vector wind speed $V_{1\text{-}10}$ and direction $\text{Dir}_{1\text{-}10}$ from 1000 ft (~0.3 km) to 10 000 ft (~3 km). Quantities are determined from the 1200 GMT Miami sounding for each day. Definitions of these quantities are given in the Appendix.

Burpee (1979) found greater amounts of midtropospheric moisture on wet sea-breeze days than on dry sea-breeze days. It is logical to assume that more rain can occur when there is more moisture to be tapped. When middle-level relative humidity was less than 50% (Table 1), only 55% (26 out of 47) of the convergence events had precipitation; average precipitation for all 47 events was 1.48 mm (2.68 mm average for the 26 rain periods). In the relative humidity range 50–65%, 28 out of 39 (72%) convergence events had rainfall, and the average was 1.77 mm per event. The best correlation ($r = -0.81$) between the change in total area divergence and rainfall is found during the latter regime. When the relative humidity is greater than 65%, 21 out of 35 convergence events have rain. As expected, the largest average area rainfall (2.19 mm) is found in this subdivision. Seven rain periods are not detected in the convergence field; average precipitation is 2.33 mm per period. One rain period with a yield of 7.33 mm is included in the seven missed rain periods, and accounts for approximately half the total undetected rain.

The Showalter stability index and *K*-index are presented because these indices have been widely used for the past 20 to 30 years as simple measures of hydrostatic instability. It appears that the Showalter stability index is not well suited for the south Florida environment. More rain occurs during higher stability periods (Table 1) than during the more unstable periods. Another parameter that incorporates low-level moisture and temperature of the entire sounding is net positive buoyant energy of a parcel. A value of 1000 J kg^{-1} was used to subdivide the ensemble in Table 1. The result is similar to that found for the stability index; slightly more rain occurs in association with weaker buoyant energy. The subtropical atmospheric temperature profile tends to be nearly moist adiabatic or weakly conditionally unstable, making the stability index and net positive buoyant energy of a parcel less effective tools for this region than for midlatitude areas.

The *K*-index is dependent not only on the temperature lapse rate and moisture content of the lower atmosphere but also on the vertical extent of the moist layer. Because of this moisture dependence, the *K*-index is a somewhat better tool for air-mass thunderstorm prediction than is the stability criterion. When the *K*-index is less than 25, only 17 out of 37 (46%) convergence events studied have precipitation. Average rainfall per event is 1.40 mm but it is 3.05 mm for the rainfall periods. The correlation coefficient between convergence and rainfall is impressive (−0.78) for *K* between 25 and 29. Thirty-five out of 42 (83%) convergence events have rain. For *K* greater than 29, only 23 of the 42 convergence events have rain for a 1.66 mm average, while the average is 3.03 mm for the 23 rain periods.

The selection of $V_{1\text{-}10}$ and $\text{Dir}_{1\text{-}10}$ as indicators of convective precipitation is based on the work of Pielke (1974) which suggests that the rainfall over the southern peninsula should be inversely correlated with wind speed. Woodley *et al.* (1982) have used $V_{1\text{-}10}$ as a variable in predictor models for estimating area precipitation. The ensemble is divided according to $V_{1\text{-}10}$ above and below 4 m s^{-1} (Table 1), the apparent dividing point between moving and stationary echoes. It is found that the weaker the wind the stronger the convergence and heavier the rainfall associated with each event. During times of weak low-level winds, 76% (35 out of 46) of the events had rainfall. Correlation coefficients are marginal, accounting for about 30% of the variance. For the strong wind regime, only 53% (40 out of 75) of the events had precipitation. When low-level direction is taken into account, more than one-third of the events (44) occurred when the average direction was between 090 and 135°. No days during the FACE 1975 field experiment had low-level directions between 270 and 360°.

Weighted convergence (defined in Section 2c) was also used to develop convergence–rainfall relationships. Weighted convergence uses only the convergence values occurring in the grid. There were 125 cases meeting the criterion of 25×10^{-6} s^{-1} or more during July and August 1975 in the FACE mesonetwork. For the total ensemble, a correlation coefficient of 0.58 was found between convergence change and rainfall amount. Seventy-three of these cases had rain, and there were 15 rain events with no associated convergence. For most of the parameters discussed above (stability, moisture and winds), weighted convergence reflects what was seen in the total area divergence relationships. In summary, although weighted convergence could be considered a more sensitive measure of convergence, it did not improve on total area divergence for this data set.

c. Timing between convergence and rainfall

Figure 4 shows the relationship between convergence events for total area divergence and rainfall as a function of time based upon certain convergence and rainfall "milestones." Shading indicates significant rain events totaling more than 1 mm area precipitation. Only the 75 rain events (Table 1) are presented. The top panel of Fig. 4 concerns times between the beginning of the convergence event and the beginning of rain. The average time is 35 min; standard deviation σ is about 31 min. The events are generally offset from zero in a positive sense, which means rain begins after initial convergence. However, some negative times occur when light precipitation begins without generating

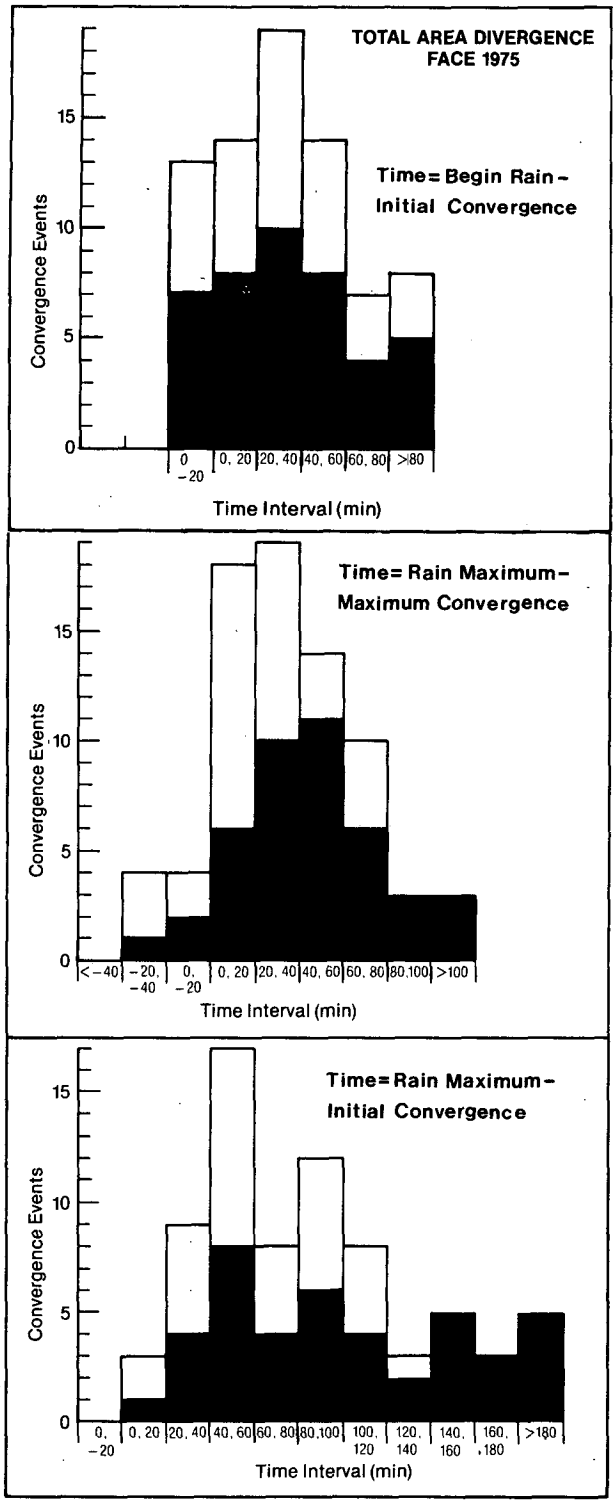

FIG. 4. Frequency distribution of convergence events relative to the time intervals between rain and convergence "milestones." Shaded blocks include events with precipitation totaling more than 1 mm.

a pulse in the total area divergence field. The initial triggering mechanism may not be detected by the grid, or the developing convection is too small to be recorded in the average field. In such a case, once precipitation begins and downdrafts are generated, the surface convergent boundaries between the initial outflow and the ambient air are revealed and recorded in the evolution of total area divergence.

The center panel of Fig. 4 concerns the time between maximum convergence and maximum rain. The average time is 38 min (σ = 35 min). Negative values indicate that the rain maximum comes before peak convergence, and show that problems can occasionally exist in objectively relating the strength of total area divergence to area precipitation. It is difficult to distinguish between periods of rain when convergence events occur within a few hours of each other.

The lower panel of Fig. 4 concerns the time between initial convergence and maximum rain. Here the average is 86 min (σ = 54 min), and in most cases a significant time interval occurs between the onset of convergence and the precipitation maximum.

In addition to identifying the periods illustrated in Fig. 4, we found that, for the July and August ensemble, the average time between initial convergence and the ending of rain was 133 min (σ = 74 min).

Figure 4 shows that there is a wide variety of convection during the study period. Times between convergence and precipitation milestones are not clustered tightly around the average, nor is there a direct correlation between time elapsed and heavier precipitation. Though much of the variability can be attributed to the highly variable nature of convection, the area-averaged technique itself, station spacing, and the location of convection relative to the mesonetwork all combine to add to the variability.

d. Convective outflow versus area rainfall

The Thunderstorm Project found that an area of heavy rain at the surface coincides with an area of strong divergence in the surface winds (Byers and Braham, 1949). The magnitude of maximum divergence was found to be directly related to the maximum rate of rainfall. When nine storms from Ohio and nine storms from Florida were analyzed, and divergence and rate of rainfall were related, correlation coefficients of 0.98 and 0.91, respectively, were identified. Cooper *et al.* (1982) found that peak area rainfall occurred approximately at the inflection point of the sinusoidal pattern of total area divergence as the area transformed from predominantly convergence to mainly divergence.

In south Florida, precipitation usually accompanies downdrafts, which in turn, cause horizontal outflow. The correlations (shown in previous sections) between initial convergence and rain are relatively low, perhaps because not all the roots of the inflow are in the surface boundary layer. Major outflows are typically seen in total area divergence and weighted divergence time series (Figs. 2a and b at 1710 EDT) as large peaks. When the area rainfall-versus-time plots are compared

with the divergence profiles, the divergence peaks are clearly related to rainfall maxima, and the larger the rain amount, the larger the divergence peak.

We identify convective outflow events by using the time series of total area divergence and weighted divergence. An outflow event for total area divergence is defined as the difference between maximum divergence and maximum convergence. In Fig. 2a, this is the period between 1535 and 1710 EDT called the "divergence event." For weighted divergence, a divergence event is described as the difference between peak divergence and the quiescent value as shown in Fig. 2b.

Table 2 presents the total area divergence statistics relating rainfall and outflow. Only the convergence events with precipitation determined in Section 3 are used. Once again, owing to the similarity between total area divergence and weighted divergence, only the statistical data for total area divergence are presented. The increase in correlation coefficients relative to those of the convergence–rainfall statistics are considerable in all categories. For the 75 rain periods, the average area rainfall is 2.87 mm; the average change in divergence is $+129 \times 10^{-6}$ s^{-1}. The correlation coefficient is $r = 0.75$, an improvement of 0.16 over the convergence–rainfall data in Table 1. When the ensemble is broken down according to the various atmospheric parameters, the correlation coefficients are quite good; only three categories are below $r = 0.70$. The maximum correlation coefficient $r = 0.89$ occurs in the K-index range of 25 to 29. When the average time between maximum outflow and rain maximum (maximum divergence − rain maximum) is determined, the time of maximum total area divergence occurs on average 20 min after the rain maximum. Maximum rain usually occurs at the inflection point (approximately 0.0 s^{-1}) in the total area divergence time series (see Fig. 2a) as the area beneath the convective system transforms from predominantly convergence to mainly divergence.

e. *Mean conditions*

The total area divergence and rainfall data for the FACE mesonetwork have been stratified into two regimes, based upon daily precipitation totals. Days during FACE 1975 with area rainfall depths totaling 3 mm or more in the mesonetwork were considered wet and those with less than 3 mm were labeled dry. 25 days were classified dry; 24 days were wet. The remaining days were not used because radar data were insufficient to estimate precipitation amounts for the entire day.

Figure 5 illustrates the daily total area divergence versus time for the 25 dry days. The familiar sinusoidal pattern (seen in Fig. 2) associated with a buildup of convergence and upward vertical motion, and divergence related to rainfall and outflow, is absent when there is only light rain or no rain in the area. Notice the relatively strong net convergence throughout the day and the maximum convergence between 1400 and 1800 EDT. The afternoon variability is quite obvious from the standard deviation. The large amounts of net convergence exhibited on most dry days are mainly a function of the location of the FACE mesonetwork. On most days, Lake Okeechobee (see Fig. 1) has a dominant influence in this region (Pielke, 1974). The lake breeze develops rather strong convergence zones

TABLE 2. Total area divergence associated with convective outflow as related to area rainfall based upon FACE 1975 mesonetwork data.

Criteria	Number of cases	$\overline{\text{Rain}}$ (mm)	$\overline{\Delta\text{DIV}}$ ($\times 10^{-6}$ s^{-1})	Correlation coefficient r	Significance
All events	75	2.87	129	0.75	<0.001
RH < 50%	26	2.68	134	0.64	<0.001
50% ≤ RH ≤ 65%	28	2.47	115	0.83	<0.001
RH > 65%	21	3.65	142	0.84	<0.001
SI > 2	39	3.15	124	0.85	<0.001
SI ≤ 2	36	2.57	134	0.56	<0.001
BE ≤ 1000 J kg^{-1}	35	3.06	137	0.77	<0.001
BE > 1000 J kg^{-1}	40	2.71	122	0.76	<0.001
KI < 25	17	3.04	161	0.63	0.006
25 ≤ KI ≤ 29	35	2.67	107	0.89	<0.001
KI > 29	23	3.03	138	0.74	<0.001
$V_{1\text{-}10} \geq 4$ m s^{-1}	40	2.36	110	0.74	<0.001
$V_{1\text{-}10} < 4$ m s^{-1}	35	3.46	150	0.76	<0.001
Dir$_{1\text{-}10}$ (360–090°)	20	3.20	123	0.79	<0.001
Dir$_{1\text{-}10}$ (090–135°)	29	3.07	139	0.78	<0.001
Dir$_{1\text{-}10}$ (135–270°)	26	2.40	122	0.71	<0.001

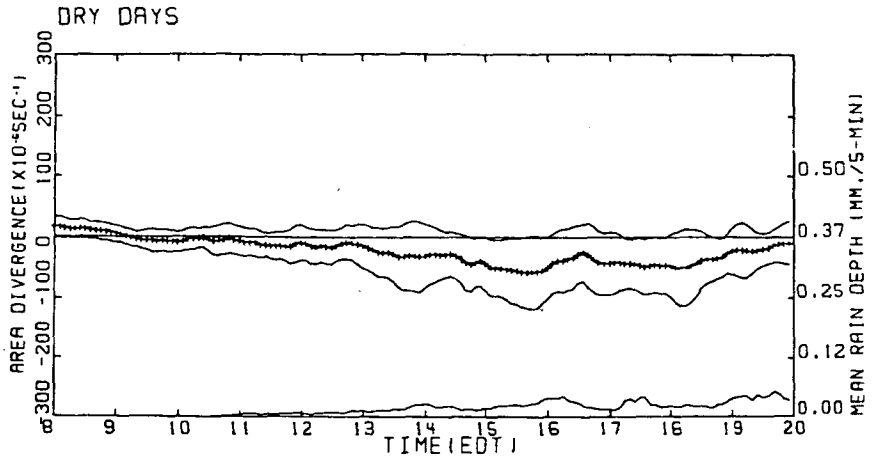

FIG. 5. Total area divergence versus time for the 25 dry days (<3 mm) during FACE 1975. One standard deviation is shown.

at the boundary of the lake outflow and the prevailing flow. The effect may or may not meet the convergence event criterion developed earlier. In another study in east-central Illinois in 1979 (Ackerman *et al.*, 1983; Watson and Holle, 1982), no-rain days exhibited very little variation in the total area divergence time profile on the meso-β scale.

Figure 6 shows the daily total area divergence and area rainfall profiles for the 24 days classed as wet. The buildup of surface convergence reaches a maximum at approximately 1330 EDT followed by a maximum in area divergence several hours later. The sinusoidal pattern is clearly evident (schematically). The maximum in rainfall agrees quite well with the crossover point (zero divergence) from negative to positive total area divergence. The divergence maximum occurs approximately 1½ hours later.

Figure 7 presents a normalized convergence event developed for south Florida. For normalization purposes, 0.0 represents beginning convergence and 1.0 is the end of the divergence or outflow. Only the 42 convergence events with area rainfall greater than 1 mm are used. The average time from begining of convergence to end of divergence is 171 min (σ = 72.5 min). The familiar sinusoidal pattern found in Figs. 2 and 6 is clearly evident (schematically). Rain begins at 0.19 of the total event, shortly before maximum convergence (0.33). A balance of convergence and divergence is found during maximum rainfall (0.60). Shortly thereafter, the maximum in divergence (0.72) is recorded in the normalized total area divergence event. As indicated by Holle and Watson (1983), it may be possible, by knowing what stage of development a convective system has reached, to determine how

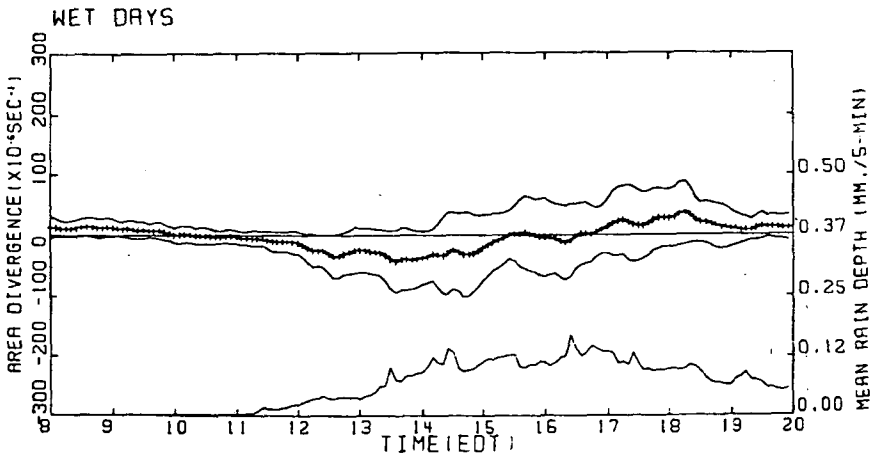

FIG. 6. Total area divergence versus time for the 24 wet days (>3 mm) during FACE 1975. One standard deviation is shown. The mean radar-derived rain depth (mm in 5 min) is presented for the same period.

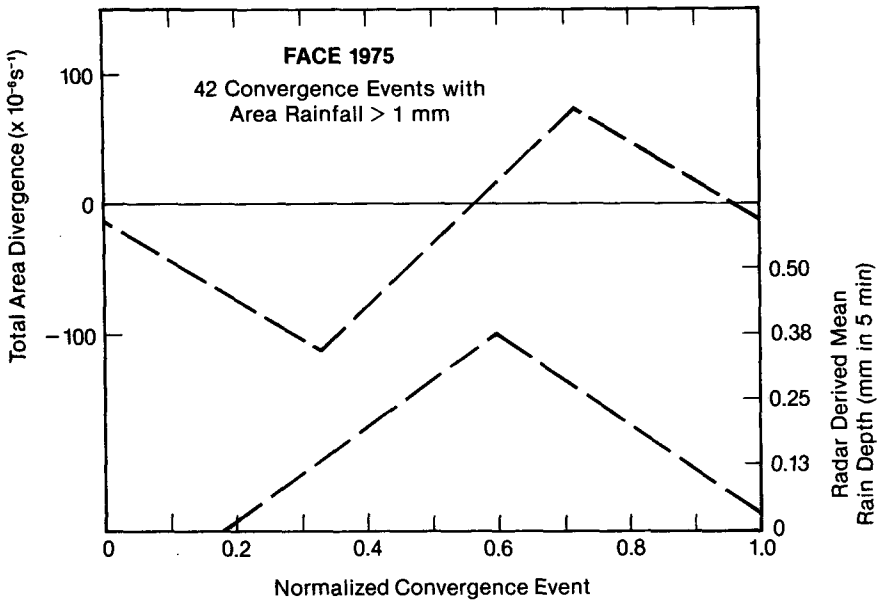

FIG. 7. Normalized convergence event for FACE 1975.

long a system will last. Total area divergence does suggest the degree of development of a particular convective system within the limits of the instrumented area.

4. Concluding remarks

The relationship between convergence on the meso-β scale and convective precipitation in south Florida has been presented. The effects of the size of the mesonetwork (Watson *et al.*, 1981) and the size and location of the convective activity (Cooper *et al.*, 1982) are critical factors in the relationship. For area divergence to have importance, the area must be equal to or somewhat larger than the convective entity being examined. The convective system is fueled from the region surrounding it and total area divergence is used to measure this process. If total area divergence were measured in an area the size of south Florida, only peninsula-scale divergence would be recorded and individual convergence and divergence cells associated with the life cycles of small or even large convective systems located over the peninsula would be lost. In a study of FACE-2 data (1978–1980), López *et al.* (1984) have found that 98% of echoes over south Florida have areas of 1500 km^2 or less. This would suggest that the FACE 1975 network (1440 km^2) is a reasonably good benchmark for such a study as this.

Our goal was to develop a methodology which is less complicated to apply than that developed on the convective scale by Ulanski and Garstang (1978). It is important to note the relative ease of treating the entire grid, as opposed to identifying and characterizing individual cells within the grid. Actually, weighted convergence, which uses only grid points with convergence, approaches the convective scale. The fact that there is little statistical difference between total area divergence and weighted convergence would imply that the results in this study approach those of Ulanski and Garstang.

Cooper *et al.* (1982) documented the linkages and feedback mechanisms present at the peninsula-, meso- and convective scales. We have quantified the strength of convergence with respect to rainfall on the network scale no matter how convection is triggered.

The question arises as to the predictive qualities of total area divergence. The results presented here are encouraging but not conclusive. For a nowcasting tool, the timing is good except for large fluctuations, as shown in Section 3c. The technique appears to work well with slow-moving convective systems that complete their life cycle within the network boundaries. The average time between beginning convergence and initial rain was 35 min; between beginning convergence and maximum rain, 86 min. It must be understood that beginning convergence could not be used as a predictive quantity. Only when there has been a steady decrease of divergence of 25×10^{-6} s^{-1} for more than 10 min, does one actually know there is a convergence event. Table 3 shows the times between certain convergence thresholds and rain milestones for FACE 1975. After a steady drop of 50×10^{-6} s^{-1}, there is an average of 13 min to initial rain; after 100×10^{-6} s^{-1}, rain has begun. However, there are still 64 min to the rain maximum. Standard deviations are quite high, emphasizing the fact that convection is highly variable.

TABLE 3. Time between total area divergence thresholds and rain milestones, based upon FACE 1975 mesonetwork data. Standard deviations are in parentheses. The number of convergence events n in each group is also shown.

Threshold	Threshold and initial rain (min)	Threshold and rain maximum (min)	Threshold and end rain (min)
Initial convergence (n = 75)	35 (31)	86 (54)	133 (74)
-25×10^{-6} s^{-1} (n = 75)	18 (30)	69 (52)	116 (73)
-50×10^{-6} s^{-1} (n = 50)	13 (32)	73 (50)	130 (71)
-75×10^{-6} s^{-1} (n = 37)	4 (31)	67 (48)	128 (63)
-100×10^{-6} s^{-1} (n = 21)	−4 (32)	64 (54)	132 (67)

If total area divergence is to be used in thunderstorm prediction, it is only one aid in the process. The use of the mesoscale surface winds and thermodynamic properties in a horizontal display can point out specific locations of convective development. Animation and overlays with radar, satellite, and lightning information complete the total mesoscale nowcasting system.

Many of the clues of convective development lie in the boundary-layer wind, temperature, and moisture fields prior to detection by satellite, radar, or lightning detectors. The use of total area divergence as described here may lead to improvement of thunderstorm prediction in terms of time, space, and intensity.

Acknowledgments. This research was supported by the Army Research Office, Department of Defense, and the Atmospheric Research Section, National Science Foundation, under NSF Grant ATM-78-08865.

Deep appreciation is extended to Bob Sax, Ron Holle, Tony Barnston, John Brown and Joe Boatman for their advice and guidance during this research effort. Appreciation is also expressed to Harry Cooper for his supervision of the data reduction effort at the University of Virginia. Many thanks go to Jeff Morris who was the focal point for data reduction at NOAA. Gratitude is also extended to all other personnel who participated in the collection of data during the FACE field effort in the summer of 1975.

APPENDIX

Glossary of Terms

Area rainfall:
Rainfall derived by radar (recorded at 5 min intervals), adjusted by a daily gage-to-radar ratio G/R and averaged over a given area.

Convergence events:
The monotonic decrease in total area divergence of more than 25×10^{-6} s^{-1} sustained for more than 10 min. The magnitude of a convergence event is the difference between the values at beginning convergence and peak convergence.

$\text{Dir}_{1\text{-}10}$ and $V_{1\text{-}10}$:
Mean vector wind speed and direction from 1000 ft (~0.3 km) to 10 000 ft (~3 km) determined from sounding data.

K-index:
The difference between the 850-mb and 500-mb temperature, plus the difference between the 850-mb dewpoint and 700-mb dewpoint depression.

Midtropospheric relative humidity:
Average relative humidity between 850 and 500 mb.

Net positive buoyant energy:
The sum of the positive buoyant energy above the level of free convection (LFC) and negative buoyant energy below the LFC. If there is no positive buoyant energy or if the net buoyant energy is negative, it is assumed zero.

Showalter stability index:
Identified by raising an air parcel at 850 mb dry-adiabatically to saturation, then moist-adiabatically to 500 mb. The magnitude is the difference between the temperature of the ambient air and that of the parcel at 500 mb.

Total area divergence:
The sum of the grid-point divergence values divided by the total number of grid points for each 5 min period.

Weighted convergence:
The sum of only negative divergence values at grid points divided by the total number of grid points for each 5-min period.

Weighted divergence:
The sum of only positive divergence values at grid points divided by the total number of grid points for each 5 min period.

REFERENCES

Ackerman, B., R. W. Scott and N. E. Westcott, 1983: Summary of the VIN field program: Summer 1979. Tech. Rep. No. 1, Illinois State Water Survey, Champaign, 105 pp.

Burpee, R. W., 1979: Peninsula-scale convergence in the south Florida sea breeze. *Mon. Wea. Rev.*, **197**, 852–860.

Byers, H. R., and R. R. Braham, Jr., 1949: *The Thunderstorm.* U.S. Govt. Printing Off., Washington, D.C., 187 pp.

——, and H. R. Rodebush, 1948: Causes of thunderstorms of the Florida peninsula. *J. Meteor.*, **5**, 275–280.

Cooper, H. J., M. Garstang and J. Simpson, 1982: The diurnal interaction between convection and peninsula-scale forcing over south Florida. *Mon. Wea. Rev.*, **110**, 486–503.

Cressman, G. P., 1959: An operational objective analysis system. *Mon. Wea. Rev.*, **87**, 367–374.

Cunning, J. B., R. L. Holle, P. T. Gannon and A. I. Watson, 1982: Convective evolution and merger in the FACE experimental area: Mesoscale convection and boundary layer interactions. *J. Appl. Meteor.*, **21,** 953–977.

Day, S., 1953: Horizontal convergence and the occurrence of summer precipitation at Miami, Florida. *Mon. Wea. Rev.*, **81,** 155–161.

Gentry, R. C., and P. L. Moore, 1954: Relation of local and general wind interaction near the sea coast to time and location of airmass showers. *J. Meteor.*, **11,** 507–511.

Holle, R. L., and A. I. Watson, 1983: Duration of convective events related to visible cloud, convergence, radar and raingage parameters in south Florida. *Mon. Wea. Rev.*, **111,** 1046–1051.

López, R. E., D. O. Blanchard, W. L. Hiscox and M. J. Casey, 1984: Population characteristics, development processes, and structure of radar echoes in south Florida. *Mon. Wea. Rev.*, **112,** 56–75.

Pielke, R. A., 1974: A three-dimensional numerical model of the sea breezes over south Florida. *Mon. Wea. Rev.*, **102,** 115–139.

Staff, Cumulus Group, 1976: 1975 Florida Area Cumulus Experiment (FACE): Operational summary. NOAA Tech. Memo. ERL WMPO-28, Boulder, 186 pp.

Tripoli, G. J., and W. R. Cotton, 1980: A numerical investigation of several factors contributing to the observed variable intensity of deep convection over south Florida. *J. Appl. Meteor.*, **19,** 1037–1063.

Ulanski, S. L., and M. Garstang, 1978: The role of surface divergence and vorticity in the life cycle of convective rainfall. Part I: Observations and analysis. *J. Atmos. Sci.*, **35,** 1047–1062.

Watson, A. I., and R. L. Holle, 1982: The relationships between low-level convergence and convective precipitation in Illinois and south Florida. Tech. Rep. No. 7, Office of Weather Research and Modification, NOAA/ERL, Boulder, and Illinois State Water Survey, Champaign, 67 pp. [NTIS AD-A127 615/3.]

——, ——, J. B. Cunning, P. T. Gannon and D. O. Blanchard, 1981: Low-level convergence and the prediction of convective precipitation in south Florida. Tech. Rep. No. 4, Office of Weather Research and Modification, NOAA/ERL, Boulder, and Illinois State Water Survey, Champaign, 228 pp. [NTIS AD-A097 553/2.]

Woodley, W. L., and A. Herndon, 1970: A raingage evolution of the Miami reflectivity–rainfall rate relationship. *J. Appl. Meteor.*, **9,** 258–263.

——, J. Jordan and A. Barnston, 1982: Rainfall results of the Florida Area Cumulus Experiment, 1970–76. *J. Appl. Meteor.*, **21,** 139–164.

——, A. R. Olsen, A. Herndon and V. Wiggert, 1975: Comparison of gage and radar methods of convective rain measurement. *J. Appl. Meteor.*, **14,** 909–928.